doi:10.1006/jmbi.2000.3995 available online at http://www.idealibrary.com on IDEAL® J. Mol. Biol. (2000) 301, 869–879

JMB

Reversible Loss of Crystallinity on Photobleaching Purple Membrane in the Presence of Hydroxylamine

Clemens Möller[1,2], Georg Büldt[2], Norbert A. Dencher[3], Andreas Engel[1] and Daniel J. Müller[1,4]*

[1]*M. E. Müller Institute for Structural Biology, Biozentrum Klingelbergstr. 70, CH-4056 Basel, Switzerland*

[2]*Forschungszentrum Jülich IBI-2, Structural Biology D-52425 Jülich, Germany*

[3]*Institut für Biochemie Physikalische Biochemie Technische Universität Darmstadt, D-64287 Darmstadt, Germany*

[4]*Max-Planck-Institute of Molecular Cell Biology and Genetics, Pfotenhauerstr. 108 D-01307 Dresden, Germany*

**Corresponding author*

Structural changes of purple membrane during photobleaching in the presence of hydroxylamine were monitored using atomic force microscopy (AFM). The process of bleaching was associated with the disassembly of the purple membrane crystal into smaller crystals. Imaging steps of the photobleaching progress showed that disassembly proceeds until the sample is fully bleached and its crystallinity is almost lost. As revealed from high resolution AFM topographs, the loss of crystallinity was initiated by loss of lattice forming contact between the individual bacteriorhodopsin trimers. The bacteriorhodopsin molecules, however, remained assembled into trimers during the entire photobleaching process. Regeneration of the photobleached sample into intact purple membrane resulted in the reassembly of the bacteriorhodopsin trimers into the trigonal lattice of purple membrane. The data provide novel insights into factors triggering purple membrane formation and structure.

Keywords: AFM; apomembrane; apoprotein; bacterioopsin; bacteriorhodopsin

Introduction

The light-driven proton pump bacteriorhodopsin (BR) oligomerizes into trimers which naturally form two-dimensional (2D) crystals in the so called purple membrane (PM) of *Halobacterium salinarum* (Blaurock & Stoeckenius, 1971). BR consists of seven transmembrane α-helices (Henderson & Unwin, 1975; Subramaniam, 1999) surrounding the photoactive retinal covalently linked to Lys216 by a Schiff base (Büldt *et al*., 1991; Jubb *et al*., 1984). Upon absorption of light the retinal isomerizes from the all-*trans* to the 13-*cis* (Oesterhelt, 1973) conformation. This triggers BR to undergo structural changes (Dencher *et al*., 1989; Edman *et al*., 1999; Koch *et al*., 1991; Luecke *et al*., 1999; Subramaniam *et al*., 1999) and the proton is transported across PM against the electrochemical gradient (Oesterhelt, 1998; Oesterhelt & Stoeckenius, 1973). Intermediates of this transport process are distinguished by their absorption maxima (Figure 1(a)). The Schiff base reacts with reagents such as hydroxylamine under illumination (Oesterhelt *et al*., 1974), and to a smaller extent in the dark (Subramaniam *et al*., 1991). This chemical reaction results in the breakage of the Schiff base bond yielding the apoprotein bacterioopsin (BO) and retinaloxime. Consequently, the absorption maximum of PM at 568 nm diminishes and an absorption maximum of retinaloxime at about 360 nm is observed (Figure 1(b); Oesterhelt *et al*., 1974). These spectral changes depend upon the illumination time and reflect the photobleaching process of PM. The loss of the Schiff base bond leads to structural changes of aromatic amino acid residues but not to an alteration of the secondary structure of the apoprotein (Bauer *et al*., 1976; Becher & Cassim, 1977). All results so far on both structural and functional properties of photobleaching BR have been obtained by measurements of PM ensembles (Becher & Cassim, 1977; Cladera *et al*., 1992; Gibson & Cassim, 1989; Hiraki *et al*., 1978; Oesterhelt *et al*., 1974; Subramaniam *et al*., 1991). Here, we describe the structural changes of photobleaching PM on the basis of individual BR molecules. Such information could reveal insights

Abbreviations used: AFM, atomic force microscopy; BR, bacteriorhodopsin; BO, bacterioopsin; PM, purple membrane.

E-mail address of the corresponding author: DANIEL.MUELLER@UNIBAS.CH

0022-2836/00/040869–11 $35.00/0

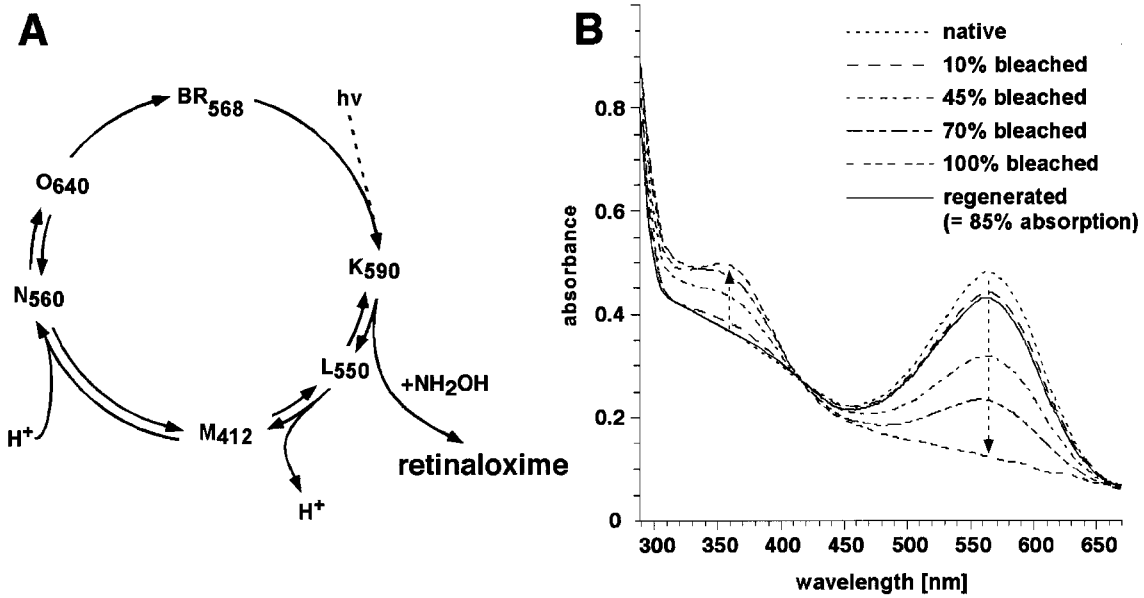

Figure 1. (a) Simplified view of the reaction of hydroxylamine during the bacteriorhodopsin (BR) photocycle (Oesterhelt, 1998; Oesterhelt *et al.*, 1974). The functional states of BR are characterized by their absorption maxima, given in indices. Upon absorption of light, the retinal undergoes an isomerization, followed by a proton release and a subsequent proton uptake. Photobleaching in the presence of hydroxylamine (NH_2OH) cleaves the Schiff base bond and takes place between intermediates K and L (Subramaniam *et al.*, 1991). (b) Absorption spectra of purple membrane (PM) upon different steps of photobleaching. Spectra were recorded from native PM, PM bleached to 10 %, 45 %, 70 % and 100 %, which corresponded to an illumination time of 5, 20, 120 and 180 minutes in hydroxylamine, respectively. The regenerated PM reached 85 % of the adsorption maximum of unbleached PM ($\lambda_{max} = 568$ nm). Bleaching buffer: 0.1 mg/ml BR, 200 mM NH_2OH (pH 7.2), 10 mM Tris-HCl.

into how individual photobleached BR molecules affect the structural appearance of PM.

The high signal-to-noise ratio of the atomic force microscope (AFM; Binnig *et al.*, 1986) allows us to observe single proteins in aqueous solution (Drake *et al.*, 1989). As demonstrated on BR (Müller *et al.*, 1995a,b, 1996, 1999a,b, 2000) and various other membrane proteins (Czajkowsky *et al.*, 1998; Fotiadis *et al.*, 1998; Hoh *et al.*, 1993; Karrasch *et al.*, 1994; Mou *et al.*, 1995; Müller & Engel, 1999; Schabert *et al.*, 1995; Scheuring *et al.*, 1999; Seelert *et al.*, 2000; Walz *et al.*, 1996; Yang *et al.*, 1993), the spatial resolution of AFM topographs is sufficient to resolve substructures of the proteins down to a few amino acid residues in size. Here we use AFM to image the structural changes of PM and of the BR assembly upon photobleaching induced breaking of the Schiff base bond of the chromophore retinal. The observed macroscopic changes are interpreted on the basis of high resolution AFM images, which allow the effect of photobleaching on individual BR molecules to be interpreted.

Results

Photobleaching of purple membrane with hydroxylamine

Absorption spectra of native PM and of PM bleached to 10 %, 45 %, 70 % and 100 % in the presence of hydroxylamine are shown in Figure 1(b). The absorption maximum of PM ($\lambda_{max} = 568$ nm) decreased with increasing illumination time, while an absorption maximum at about 360 nm appeared. These spectral changes reflect the conversion of BR to BO and to retinaloxime which remains attached to the membrane (Bauer *et al.*, 1976; Oesterhelt *et al.*, 1974). PM was bleached completely after an illumination time of ≈180 minutes (Figure 1(b)). If illuminated in the absence of hydroxylamine for more than 24 hours PM did not show changes in the absorption spectra (data not shown). The completely photobleached sample was regenerated in the dark in the presence of all-*trans* retinal for three hours. The regenerated PM (Figure 1(b), curve 6) had 85 % of the absorption maximum observed for unbleached PM.

Structural changes of photobleached purple membrane

After photobleaching to 10 % the PM exhibited cracks dividing the crystalline patches into smaller crystalline areas (Figure 2(a) and (e)). The cracks had lengths up to a few hundred nm and separated the crystalline areas by about 5 to 15 nm. As revealed by height analyses, the maximum height difference between the protein surface and the surface of the gap was 1.2(±0.5) nm ($n = 30$); considering the height of native PM, 5.6 nm (Müller *et al.*, 1999a) the cracks separating the crystalline patches exhibited a height of ≈4.4 nm. Thus, the space

beteween the proteins was most likely filled with a lipid bilayer. The formation of cracks and the division of PM into smaller crystalline patches increased with the illumination time (Figure 2(b), (c), (f) and (g)). It should be noted here, that the formation of cracks was observed on both PM surfaces. Completely bleached PM almost lost the crystalline assembly of the proteins (Figure 2(h)). Occasionally, small crystalline areas a few tens of nanometers in diameter were observed. The disappearance of PM crystallinity during photobleaching is also observed by the power spectra (Figure 2(i), (j), (k), and (l)) of the high resolution topographs (Figure 2(e), (f), (g), and (h)), respectively. With progress of photobleaching the spots of the power spectra smeared out and the diffraction rings broadened and disappeared. In contrast to the disappearance of the crystallinity, the diameter of the PM (between 400 and 1500 nm) remained essentially unchanged during the entire photobleaching process (Figure 2(a)-(d)).

Assembly of bacterioopsin in photobleached purple membrane

To be able to interpret the observed loss of crystallinity on the scale of individual BR molecules, we recorded high resolution topographs of the photobleaching process (Figures 3 and 4). PM photobleached to 45% showed structurally well preserved BR trimers which were assembled into crystalline patches. These crystalline areas were separated by cracks. After cross-correlation with a protein trimer, the positions of most trimers were marked (Figure 3(b)), demonstrating that, the trigonal lattice of the trimers was roughly preserved within small areas of a patch (Figure 3, centre of area I). The crystalline orientation of BR trimers separated by several tens of nanometers deviated by a small degree (Figure 3(b), top left of areas I and II). Consequently, a shift of the lattice lines could be observed even within single membrane patches (Figure 3(b), area II). Extending to the crystalline lattice of area I towards the neighbouring crystal patch further demonstrated that the orientation of the patches relative to each other was lost upon crack formation.

In completely photobleached PM, the crystalline assembly of the BO trimers was strongly distorted (Figure 4). Occasionally, small crystalline areas with diameters of a few unit cells were observed while most of the BO trimers lost their crystalline orientation (Figure 4(b)). As documented above, the lattices of such micro crystals were rotated with respect to each other by a few degrees. The three subunits of the cytoplasmic BO trimer surface featured three particularly pronounced protrusions extending 0.7($\pm$0.1) nm ($n = 140$) above the lipid surface, which was close to the 0.8($\pm$0.1) nm found for native PM (Müller *et al.*, 1999a). As shown previously, these protrusions arise from polypeptide loops connecting transmembrane α-helices E and F. Depending on the variation of the applied force, the prominent E-F loop can be bent away and the shorter loops of the BO monomer can be visualized (Müller *et al.*, 1995b). This conformational change is fully reversible, suggesting that loop E-F is a rather flexible element on the cytoplasmic surface of the native BR molecule (Heymann *et al.*, 1999). Furthermore, this effect explains the structural variations of the BO trimers observed within one topograph.

To gain solid information about the cytoplasmic surface structure of the apoprotein, topographs of 680 BO trimers were selected, aligned translationally and rotationally by correlation with a well preserved particle and averaged. The 3-fold symmetrized correlation average shows the three peripheral protrusions of the BO trimer more clearly (Figure 4(a), inset). Comparing the surface structures of the BO trimer to those obtained at a similar resolution of 0.8 nm from BR trimers (Müller *et al.*, 1995b) showed no structural differences.

Regeneration of photobleached purple membrane

Upon addition of all-*trans* retinal, BO reforms a Schiff base bond with the retinal. The successful regeneration of photobleached membrane was monitored by the absorption spectra which was similar to that of native BR (Figure 1(b)). The regenerated membranes adsorbed flatly onto freshly cleaved mica (Figure 5(a)) exhibiting an average diameter between 400 and 1500 nm and an average height of 5.8($\pm$0.8) nm ($n = 55$). These values were in agreement with those measured on native PM (Müller & Engel, 1997).

Topographs of the regenerated extracellular BR surface revealed the arrangement of tripartite protrusions on a trigonal lattice of 6.2($\pm$0.4) nm side length (Figure 5(b)). The maximum height difference between the protein and the lipid membrane was 0.5($\pm$0.1) nm ($n = 52$). Averaged and 3-fold symmetrized topographs showed the tripartite morphology of three major domains arranged on an equilateral triangle and three minor domains per BR trimer (Figure 5(b), inset). Comparing the average to the analogous set obtained under similar buffer conditions on native PM showed an excellent structural correlation (Müller *et al.*, 1999a).

The cytoplasmic BR surface imaged with a force of 100 pN applied to the AFM stylus revealed trimeric structures arranged in a trigonal lattice of 6.2($\pm$0.4) nm side length (Figure 5(c)). Each BR molecule in the trimer featured a particularly pronounced protrusion extending 0.7($\pm$0.3) nm ($n = 32$) above the lipid surface. Correlation averaging and 3-fold symmetrization enhanced the structure of the BR trimer (Figure 5(c), inset). This structure was in good agreement with topographs on the cytoplasmic surface of native PM recorded under similar conditions (Müller *et al.*, 1999a; compare also Figure 4(a), inset).

Figure 2 (*legend opposite*)

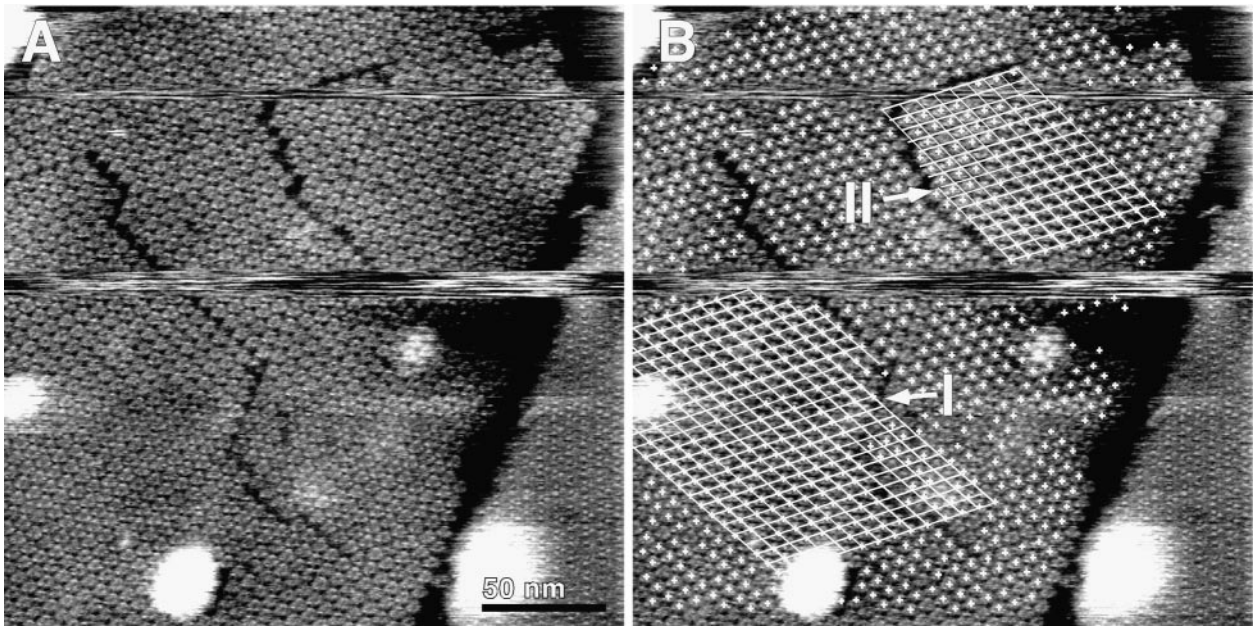

Figure 3. PM photobleached to 45 %. (a) Topograph of the cytoplasmic membrane surface. (b) Topograph with correlation peak maxima of the trimers indicated by crosses ($n = 881$) and crystal lattices drawn. Imaging buffer: 150 mM KCl (pH 7.8), 10 mM Tris-HCl. Vertical full gray level range, 1.2 nm.

Discussion and Conclusions

Disassembly of photobleached purple membrane

Photobleaching of PM in the presence of hydroxylamine leads to a loss of the Schiff base bond between retinal and Lys216 of BR. The AFM topographs presented here allowed us to follow structural changes of the BR assembly associated with photobleaching. Initial steps of photobleaching PM showed the disassembly of the PM crystal into smaller crystalline patches. The crystalline patches had no direct connection to adjacent patches and, thus, their lattices were rotated relative to each other to a small degree. The areas between the crystal patches that had no discernible structural features exhibited a thickness of 4.4 nm, similar to the 4.3 nm measured for the lipid bilayer of native PM (Müller *et al.*, 1999a). Hence, the material of these areas embedding the crystalline patches most likely represented lipid bilayer regions without protein. At advanced photobleaching the size of the crystalline areas further decreased. As a consequence of this disassembly, entirely bleached PMs almost completely lost their crystallinity (Figures 2(h) and 4). In cases where the cracks did not separate the protein crystal entirely (Figure 3), it was observed that cracked areas tend to separate although the crystals were still connected at some areas. Hence, we assume that there might be a repulsive interaction that separates the photobleached proteins.

To ensure that the observed structural changes are the result of the cleavage of the Schiff base bond we illuminated an analogous set of PM in the absence of hydroxylamine. We could not observe spectroscopic or structural changes of these samples (data not shown). To confirm that the disassembly of photobleached PM is not effected by the adsorption of apomembranes onto mica we recorded transmission electron microscopy images of negatively stained specimens (Bremer *et al.*, 1992). Although the signal-to-noise ratio of the electron microscope was not sufficient to observe individual crystalline cracks the hexagonal diffraction pattern of the protein membrane smeared out with advanced photobleaching (data not shown). This supports our observation that photobleached PM disassembles into randomly oriented smaller crystals until the crystallinity is completely lost.

Figure 2. AFM topographs of progressively photobleached PM. Images (a), (b), (c) and (d) were recorded in the deflection mode, topographs (e), (f), (g) and (h) were recorded in the height mode. Images were recorded on PM bleached to 10 % ((a) and (e)), on PM bleached to 45 % ((b) and (f)), on PM bleached to 70 % ((c) and (g)) and on PM bleached to 100 % ((d) and (h)). Figures (i), (j), (k) and (l) present power spectra (left of each Figure) and circular symmetrized power spectra (right of each Figure) of topographs (e), (f), (g) and (h), respectively. Imaging buffer: 150 mM KCl, (pH 7.8), 10 mM Tris-HCl ((a), (b), (e), (f), and (h)) and 300 mM KCl (pH 7.8), 10 mM Tris-HCl ((c), (d), and (g)). Vertical full gray level ranges 1.6 nm ((a), (b), (c), and (d)), and 1.2 nm ((e), (f), (g), and (h)).

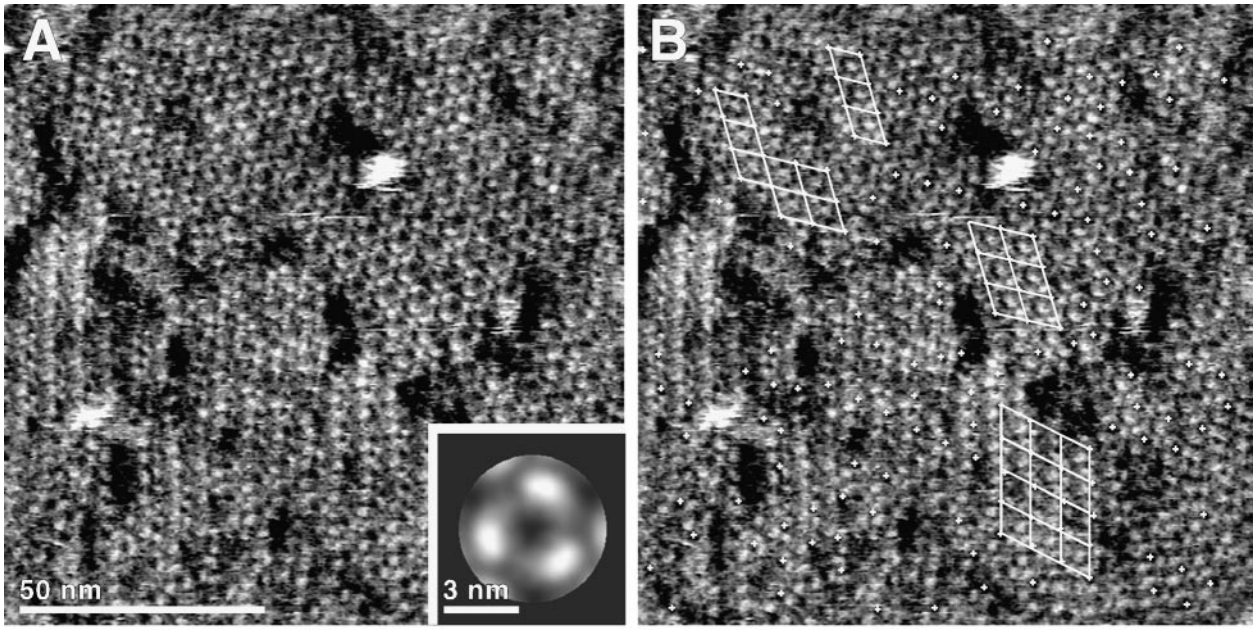

Figure 4. PM photobleached to 100 %. (a) Topograph of the cytoplasmic membrane surface. The 3-fold symmetrized correlation average of the BR trimer ($n = 172$) is shown in the inset. (b) Topograph with correlation peak maxima indicated by crosses ($n = 172$) and crystal lattices drawn. Imaging buffer: 150 mM KCl (pH 7.8), 10 mM Tris-HCl. Vertical full gray level range, 1.2 nm.

Hydroxylamine enters purple membrane from both surfaces

To answer the question whether hydroxylamine preferably enters PM from either the cytoplasmic or the extracellular surface, photobleaching was performed (in 200 mM hydroxylamine, pH 7.2, 20 mM Tris-HCl) on PM which had been adsorbed with random orientation onto mica (Müller *et al*., 1996). Since either one or the other PM surface was in contact with the mica, we assume that hydroxylamine only penetrates into PM from the surface directed towards the aqueous solution. However, the AFM topographs of photobleached PM showed structural changes of both membrane surfaces which were identical with those observed for PM photobleached in suspension (data not shown). This finding indicates that hydroxylamine diffuses into the membrane leaflets from both PM surfaces to break the Schiff base bond under illumination.

Photobleached bacteriorhodopsin remains stably assembled into trimers

It was possible to observe structural changes of the photobleaching process on the scale of individual proteins. The crystalline areas of photobleached PM showed a poor order (Figure 3). Protein trimers within one crystalline patch but separated by a few tens of nanometers were slightly rotated relative to each other. As can be directly seen from individual protein trimers located at crystal edges (Figures 3(a) and 4(b)), the disassembly into smaller crystalline patches was initiated by the loss of the lipidic trimer to trimer contacts. Obviously, the conversion of BR into BO and retinaloxime changed the lipid-mediated interactions between the protein trimers which disassembled the 2D crystal. Interestingly, the photobleached BR trimer itself did not disassemble into BO monomers.

In previous measurements, the retinal molecule and particularly the protonated Schiff base were found to be compacting elements for BR (Cladera *et al*., 1992). Our results suggest that the transformation of BR into BO changes the interactions between the trimers but to a lesser extent within the trimer. The breakage of the Schiff base bond results in subtle changes of the protein structure (Bauer *et al*., 1976). Since the BR trimer remains stable during the entire course of photobleaching (Figure 4), we conclude that these structural changes occur at the transmembrane outer rim of the trimer, which is formed by helices A, E, F, and by helix G to which the retinal is bound. Such structural changes would influence the lipid-mediated interaction between adjacent trimers. These findings agree favourably with the prediction from molecular dynamics simulation of the binding pathway of retinal to bacterioopsin. A window between helices E and F in the transmembrane part was identified as an entry point of the retinal (Isralewitz *et al*., 1997).

As reported recently, the conformation of the flexible EF loop depends on the interactions with the environment (Heymann *et al*., 1999). For example, helix-helix interactions between BR molecules were found to influence the loop structure (Müller *et al*., 1999a). Therefore, one would expect that the EF loop changes its structure upon

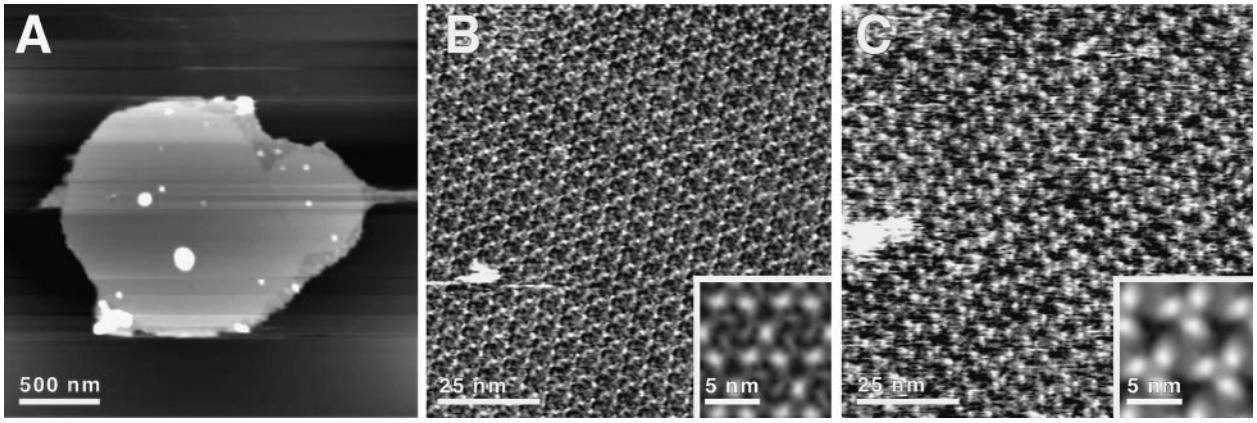

Figure 5. Topographs of regenerated bacteriorhodopsin. (a) Overview of a membrane flatly adsorbed onto freshly cleaved mica. (b) Topograph of the extracellular surface. The inset shows the 3-fold symmetrized correlation average of (b). (c) Topograph of the cytoplasmic surface. The inset shows the 3-fold symmetrized correlation average of (c). Imaging buffer: 150 mM KCl (pH 7.8), 10 mM Tris-HCl. Vertical full gray level ranges, 20 nm in (a), 1.2 nm in (b) and (c), and 1 nm in the insets.

removal of the chromophore. Surprisingly, the pronounced EF loop protrusions observed of the BO trimer (Figure 4(a)) showed no differences to those obtained on the BR trimer when imaged at a lateral resolution of 0.8 nm and a vertical resolution of ≈0.1 nm. Thus, we conclude that the structural changes upon chromophore removal were subtle and did not significantly influence the orientation of the transmembrane α-helices E and F to which the loop is connected.

Interestingly, calorimetric and X-ray diffraction studies of PM (Hiraki *et al*., 1981; Jackson & Sturtevant, 1978) disclose two thermal transitions which depend on the humidity of the sample: a reversible transition around 80 °C with a denaturation enthalpy of $H = 8$ kcal/mol and an irreversible transition around 100 °C with $H = 100$ kcal/mol. The general picture that emerges from these studies is that BR monomers reversibly change their conformation at 80 °C, causing dissociation of the lattice into a dispersion of BR trimers. At around 100 °C, the BR trimers dissociate into monomers and denature, which is accompanied by irreversible unfolding (Müller *et al*., 2000). Thus the energy to dissociate BR trimers is by a factor of 12 higher than the energy required to dissociate the lattice of PM. The most important feature of denaturing BR molecules is the dissociation of the BR trimer into monomers. BR trimers are stabilized by interactions mainly between helices B and D and to a lesser extent between helices A and E of adjacent BR molecules forming the trimer (Essen *et al*., 1998; Haltia & Freire, 1995; White & Wimley, 1999). Clearly, the energy transferred by the cleavage of the Schiff base bond is not sufficient to destabilize these interactions.

The AFM topographs show a wide variation of the distance between individual photobleached BR trimers (Figure 4). Such an effect can also be documented by the power spectra (Figure 2(i) to (l)) of the topographs. The first order peak characterizing the 6.2 nm lattice distance of the BR trimers broadens in accordance to the loss of the crystal lattice. The full width at half maximum of this diffraction ring (Figure 2(l)) indicates the distribution of lateral distance between the bleached BR trimers to be 7.2(±1.0) nm. These direct (AFM topographs) and indirect (power spectra) observations of the disassembly process are in agreement with X-ray scattering data obtained from apo-brown (Hiraki *et al*., 1978), deionized blue (Heyn *et al*., 1989) and photobleached (Hiraki *et al*., 1981) PM. In these measurements, the diffraction rings characterizing the crystallinity of the sample broadened and smeared out. However, most of the high resolution diffraction rings that correspond to the substructure of BR trimer and of BR molecules showed minor changes. These results indicate that the secondary structure of BR did not change upon bleaching and that structural changes responsible for the disassembly of the PM lattice are minimal.

Relevance of the de- and re-crystallization to other 2D crystals

Naturally BR assembles into 2D crystals by a process of self aggregation (Henderson, 1977; Neugebauer *et al*., 1978). As is the case for most other membrane proteins that form artificial 2D crystals (Engel *et al*., 1992; Hasler *et al*., 1998; Jap *et al*., 1992), the lipid composition of the membrane is essential for the crystallization. Our experiments carry novel insights into this finding: Photobleaching changes the interaction between the BR trimers and the PM lattice disassembles. Regeneration of the retinal chromophore leads to a spontaneous recrystallization of the BR trimers into a trigonal crystal (Figure 5) indistinguishable from that of native PM (Müller *et al*., 1999a). From the observation that the arrangement of the BR monomers remains trimeric upon photobleaching, it becomes clear that the protein symmetry and the lipid environment are not the only factors determining whether a two-dimensional crystallization occurs.

Apparently the protein-lipid interactions are also essential for crystal assembly Our finding indicates that specific protein-lipid interactions must exist within PM (Sternberg *et al*., 1989), which is in agreement with recent electron microscopy and X-ray diffraction data of BR (Belrhali *et al*., 1999; Essen *et al*., 1998; Grigorieff *et al*., 1996; Luecke *et al*., 1999; Sato *et al*., 1999).

Relevance to the biosynthesis of purple membrane

During biosynthesis the characteristic spectroscopic and structural properties of PM are only observed after the formation of BR from BO and retinal (Sumper & Herrmann, 1976 a,b). In this work, the reversal of this process was studied: we cleaved the Schiff base bond between the retinal and BR in the presence of hydroxylamine and light and studied the structural changes of PM. BR remained stably assembled into trimers which lost their orientation within the PM lattice. From these observations, we conclude that BO is able to form trimers without the need for retinal. After replacement of the retinaloxime with retinal the Schiff base bond was re-established and the BR trimers spontaneously re-assembled into membrane patches exhibiting a two-dimensional trigonal lattice. These crystalline membrane patches were structurally and spectroscopically indistinguishable from native PM.

Similarities between bacteriorhodopsin and rhodopsin

BR as a light-driven proton pump and rhodopsin as a light-activated G-protein coupled receptor share important features (Helmreich & Hofmann, 1996; Henderson *et al*., 1990). Both molecules contain seven transmembrane α-helices, that surround the chromophore. The retinal is covalently linked by a Schiff base bond to a lysine residue, at the centre of the seventh helix. Signal transduction of rhodopsin is initiated after absorption of a photon by the isomerization of the 11-*cis* retinal to the all-*trans* retinal. The corresponding helix F is seen to move upon isomerization, opening an unbinding/binding pathway of the retinal (Farrens *et al*., 1996). This conformational change is followed by the disintegration of rhodopsin into the apoprotein opsin and retinal. Attempts to crystallize rhodopsin yielded diffracting 2D crystals and the structure of bovine rhodopsin was resolved to 0.5 nm using cryo-electron microscopy (Krebs *et al*., 1998; Unger *et al*., 1997). Interestingly, isomerization of the retinal with its concomitant dissociation from rhodopsin is followed by a loss of the crystalline order (personal communication, G.F.X. Schertler, Cambridge, UK). Thus, BR and vertebrate rhodopsin have in common that helices E, F and G (corresponding to rhodopsin helices 5, 6 and 7) after removal of the retinal undergo structural changes affecting the lipid-mediated interaction between the apoproteins.

The common motif of seven transmembrane α-helices constitutes a large group of membrane proteins including ion pumps in archaebacteria and G-protein coupled receptors in eukaryotes. The availability of the structure of the closely related photo-activated proton pump BR, allowed us to explore interactions on the molecular scale. This study forms the basis for future studies to unravel the complicated interactions of rhodopsin. Our next experiments will focus on the interaction of bleached rhodopsin (opsin) to adjacent rhodopsins. Knowledge of the effects of studying such interactions in different contexts (Heymann *et al*., 2000) will allow us to observe how individual G-protein coupled receptors interact with other molecules.

Materials and Methods

Purple membrane

PM of *Halobacterium salinarum* strain ET1001 was isolated as described by Oesterhelt & Stoeckenius (1974). The membranes were frozen and stored at −70 °C. After thawing, stock solutions (10 mg protein/ml) were kept in ultra pure water (>18 MOhm/cm; Branstead, Boston, MA) at 4 °C.

Photobleaching

Photobleaching was performed in a tube containing PM (10 μg/ml), with 200 mM hydroxylamine (pH 7.2, 20 mM Tris-HCl). The sample-containing tube was cooled in a water bath at room temperature and illuminated using a 150 W (Halogen lamp, with heat filter) slide projector. After an illumination time of 5, 20, 120, and 180 minutes, aliquots of the sample were characterized by their absorption (Figure 1(b)) spectra and by AFM. Photobleaching, spectroscopy and AFM measurements were performed within one day. Bleaching of PM adsorbed to mica was performed as described above.

For regeneration, bleached membranes were centrifuged several times at 10,000 *g* and washed with ultra pure water to remove the hydroxylamine. After this, a slight excess of all-*trans* retinal (0.01 M) in an ethanolic solution (⩽1 %) was added in the dark (Oesterhelt *et al*., 1974) and allowed for insertion into BO for three hours. Before recording absorption spectra and AFM topographs the sample was centrifuged and washed with ultra pure water several times as described above. All buffers were made with ultra pure water. Chemicals were grade p.a., and purchased from Sigma AG (Buchs, Switzerland). Absorption spectra were recorded using the Hewlett Packard photometer HP8453 UV-Visible Spectroscopy System and ChemStation.

AFM

Instrumentation

A commercial AFM (Nanoscope III, Digital Instruments, Santa Barbara, CA) equipped with either a 15 μm D-scanner or a 120 μm J-scanner and a fluid cell was used in contact mode. Before use, the fluid cell was cleaned with conventional dish cleaner, and rinsed several times with ultra pure water and ethanol. Muscovite

Mica (Mica New York corp., New York, USA) was punched to a diameter of about 6 mm and glued onto a 12 mm Teflon disc with water-insoluble epoxy glue (Araldit, Novartis, Basel, Switzerland). The Teflon disc was glued onto a slightly smaller steel disc to allow magnetic fixing of the sample onto the piezo scanner. V-shaped cantilevers, having oxide sharpened Si_3N_4 tips, were purchased from Olympus Ltd. (Tokyo, Japan) and had a length of 120 μm, and a nominal force constant of $k = 0.1\ N/m$.

Sample preparation

The sample was diluted to a final concentration of about 0.1 mg/ml (protein) in 300 mM KCl (pH 7.8, 10 mM Tris-HCl) and a drop of 20 μl was placed onto freshly cleaved mica. After adsorption for 15 minutes, the sample was gently washed with buffer solution to remove weakly attached membrane patches (Müller *et al*., 1997).

Imaging

Before engaging, the scan size and the offset of the microscope were set to 0 to minimize sample deformation and contamination of the tip. At low magnification (frame size >500 nm), contact mode imaging was performed in the error signal mode acquiring height and deflection signal simultaneously (Putman *et al*., 1992). Gains and scan speed were optimized to minimize the deflection signal. At high magnification, topographs were recorded in trace and retrace direction simultaneously to identify and eliminate scan artifacts. The scan speed was roughly linear to the scan size, ≈four lines per second for lower magnification (512 pixel/line, frame size 1 to 25 μm), and up to 8 Hz for high magnification (frame size down to 100 nm). To achieve subnanometer resolution, the electrolyte was adjusted to control the tip-sample interactions (Müller *et al*., 1999b). Best imaging conditions were found to be between 150 mM and 250 mM KCl (pH 7.8, 10 mM Tris-HCl). While recording the topograph, the applied force was corrected manually (⩽100 pN) to compensate for thermal drift.

Image processing

Raw data topographs (512 × 512 pixel) were selected by comparing height profiles acquired in trace and retrace directions, and transferred to a digital VAX station. Only topographs showing no significant differences between both scan directions were subjected to image processing using the SEMPER image processing system (Saxton *et al*., 1979). To determine positions of the BR trimers, we calculated cross-correlation maxima between a well preserved unit cell and the topographs (Saxton & Baumeister, 1982). Crystal lattices were drawn using the correlation peak coordinates. Correlation averages were calculated using the cross-correlation maxima. The resulting correlation average was used as reference for refinement cycles until the final average was 3-fold symmetrized.

Acknowledgements

We thank Christian Baeken and Dr Joachim Heberle for preparing some of the photobleached samples, Dr Shirley Müller for critical reading of the manuscript and Dr Martin Weik for stimulating discussions. This work was supported by the Swiss National Foundation for Scientific Research, the Maurice E. Müller Foundation of Switzerland, the Sonderforschungsbereich SFB (189 and 472) of the Deutsche Forschungsgemeinschaft.

References

Bauer, P.-J., Dencher, N. A. & Heyn, M. P. (1976). Evidence for chromophore-chromophore interactions in the purple membrane from reconstitution experiments of the chromophore-free membrane. *Biophys. Struct. Mech.* **2**, 79-92.

Becher, B. & Cassim, J. Y. (1977). Effects of bleaching and regeneration on the purple membrane structure of *Halobacterium halobium*. *Biophys. J.* **19**, 285-297.

Belrhali, H., Nollert, P., Royant, A., Menzel, C., Rosenbusch, J. P., Landau, E. M. & Pebay-Peyroula, E. (1999). Protein, lipid and water organization in bacteriorhodopsin crystals: a molecular view of the purple membrane at 1.9 Å resolution. *Struct. Fold. Des.* **7**, 909-917.

Binnig, G., Quate, C. F. & Gerber, C. (1986). Atomic force microscope. *Phys. Rev. Letters,* **56**, 930-933.

Blaurock, A. E. & Stoeckenius, W. (1971). Structure of the purple membrane. *Nature New Biol.* **233**, 152-154.

Bremer, A., Henn, C., Engel, A., Baumeister, W. & Aebi, U. (1992). Has negative stain still a place in biomacromolecular electron microscopy? *Ultramicroscopy,* **46**, 85-111.

Büldt, G., Konno, K., Nakanishi, K., Ploehn, H. J., Rao, B. N. & Dencher, N. A. (1991). Heavy-atom labelled retinal analogues located in bacteriorhodopsin by X-ray diffraction. *Photochem. Photobiol.* **54**, 873-879.

Cladera, J., Galisteo, M., Sabes, M., Mateo, P. & Padros, E. (1992). The role of retinal in the thermal stability of the purple membrane. *Eur. J. Biochem.* **207**, 581-585.

Czajkowsky, D. M., Sheng, S. & Shao, Z. (1998). Staphylococcal α-Hemolysin can form hexamers in phospholipid bilayers. *J. Mol. Biol.* **276**, 325-330.

Dencher, N. A., Dresselhaus, D., Zaccai, G. & Büldt, G. (1989). Structural changes in bacteriorhodopsin during proton translocation revealed by neutron diffraction. *Proc. Natl Acad. Sci. USA,* **86**, 7876-7879.

Drake, B., Prater, C. B., Weisenhorn, A. L., Gould, S. A. C., Albrecht, T. R., Quate, C. F., Cannell, D. S., Hansma, H. G. & Hansma, P. K. (1989). Imaging crystals, polymers, and processes in water with the atomic force microscope. *Science,* **243**, 1586-1588.

Edman, K., Nollert, P., Royant, A., Belrhali, H., Pebay-Peroula, E., Hajdu, J., Neutze, R. & Landau, E. M. (1999). High-resolution X-ray structure of an early intermediate in the bacteriorhodopsin photocycle. *Nature,* **401**, 822-826.

Engel, A., Hoenger, A., Hefti, A., Henn, C., Ford, R. C., Kistler, J. & Zulauf, M. (1992). Assembly of 2-D membrane protein crystals: dynamics, crystal order, and fidelity of structure analysis by electron microscopy. *J. Struct. Biol.* **109**, 219-234.

Essen, L.-O., Siegert, R., Lehmann, W. D. & Oesterhelt, D. (1998). Lipid patches in membrane protein oligomers: crystal structure of the bacteriorhodopsin-lipid complex. *Proc. Natl Acad. Sci. USA,* **95**, 11673-11678.

Farrens, D. L., Altenbach, C., Yang, K., Hubbell, W. L. & Khorana, H. G. (1996). Requirement of rigid-body

motion of transmembrane helices for light activation of rhodopsin. *Science,* **274**, 768-770.

Fotiadis, D., Müller, D. J., Tsiotis, G., Hasler, L., Tittmann, P., Mini, T., Jenö, P., Gross, H. & Engel, A. (1998). Surface analysis of the photosystem I complex by electron and atomic force microscopy. *J. Mol. Biol.* **283**, 83-94.

Gibson, N. J. & Cassim, J. Y. (1989). Nature of forces stabilizing the transmembrane protein bacteriorhodopsin in purple membrane. *Biophys. J.* **56**, 769-780.

Grigorieff, N., Ceska, T. A., Downing, K. H., Baldwin, J. M. & Henderson, R. (1996). Electron-crystallographic refinement of the structure of bacteriorhodopsin. *J. Mol. Biol.* **259**, 393-421.

Haltia, T. & Freire, E. (1995). Forces and factors that contribute to the structural stability of membrane proteins. *BBA-Bioenergetics,* **1228**, 1-27.

Hasler, L., Heymann, J. B., Engel, A., Kistler, J. & Walz, T. (1998). 2D crystallization of membrane proteins: rationales and examples. *J. Struct. Biol.* **121**, 162-171.

Helmreich, E. J. M. & Hofmann, K.-P. (1996). Structure and function of proteins in G-protein coupled signal transfer. *Biochem. Biophys. Acta,* **1286**, 285-322.

Henderson, R. (1977). The purple membrane from *Halobacterium halobium*. *Annu. Rev. Biophys. Bioeng.* **6**, 87-109.

Henderson, R. & Unwin, P. N. T. (1975). Three-dimensional model of purple membrane obtained by electron microscopy. *Nature,* **257**, 28-32.

Henderson, R., Shertler, F. R. S. & Shertler, G. F. X. (1990). The structure of bacteriorhodopsin and its relevance to the visual opsins and other seven-helix G-protein coupled receptors. *Phil. Trans. Roy. Soc. Lond.* **326**, 379-389.

Heymann, J. B., Müller, D. J., Landau, E., Rosenbusch, J., Pebay-Peroulla, E., Büldt, G. & Engel, A. (1999). Charting the surfaces of purple membrane. *J. Struct. Biol.* **128**, 243-249.

Heymann, J. B., Pfeiffer, M., Hildebrandt, V., Fotiadis, D., de Groot, B., Kabak, R., Engel, A., Oesterhelt, D. & Müller, D. J. (2000). Conformations of the rhodopsin third cytoplasmic loop grafted onto bacteriorhodopsin. *Structure,* **8**, 643-644.

Heyn, M. P., Dudda, C., Otto, H., Seiff, F. & Wallat, I. (1989). The purple to blue transition of bacteriorhodopsin is accompanied by a loss of the hexagonal lattice and a conformational change. *Biochemistry,* **28**, 9166-9172.

Hiraki, K., Hamanaka, T., Mitsui, T. & Kito, Y. (1978). Formation of the two-dimensional hexagonal lattice of bacteriorhodopsin in reconstituted brown membranes. *Biochim. Biophys. Acta,* **536**, 318-322.

Hiraki, K., Hamanaka, T. & Kito, Y. (1981). Phase transitions of the purple membrane and the brown halo-membrane: X-ray diffraction, circular dicroism spectrum and absorption spectrum studies. *Biochim. Biophys. Acta,* **647**, 18-28.

Hoh, J. H., Sosinsky, G. E., Revel, J.-P. & Hansma, P. K. (1993). Structure of the extracellular surface of the gap junction by atomic force microscopy. *Biophys. J.* **65**, 149-163.

Israelewitz, B., Izrailev, S. & Schulten, K. (1997). Binding pathway of retinal to bacterio-opsin: a prediction by molecular dynamics simulations. *Biophys. J.* **73**, 2972-2979.

Jackson, M. B. & Sturtevant, J. M. (1978). Phase transitions of the purple membrane of the *Halobacterium halobium*. *Biochemistry,* **17**, 911-915.

Jap, B. K., Zulauf, M., Scheybani, T., Hefti, A., Baumeister, W., Aebi, U. & Engel, A. (1992). 2D crystallization: from art to science. *Ultramicroscopy,* **46**, 45-84.

Jubb, J. S., Worcester, D. L., Crespi, H. L. & Zaccai, G. (1984). Retinal location in purple membrane of *Halobacterium halobium*:a neutron diffraction study of membranes labeled *in vivo* with deuterated retinal. *EMBO J.* **3**, 1455-1461.

Karrasch, S., Hegerl, R., Hoh, J., Baumeister, W. & Engel, A. (1994). Atomic force microscopy produces faithful high-resolution images of protein surfaces in an aqueous environment. *Proc. Natl Acad. Sci. USA,* **91**, 836-838.

Koch, M. H. J., Dencher, N. A., Oesterhelt, D., Plöhn, H.-J., Rapp, G. & Büldt, G. (1991). Time-resolved X-ray diffraction study of structural changes associated with the photocycle of bacteriorhodopsin. *EMBO J.* **10**, 521-526.

Krebs, A., Villa, C., Edwards, P. C. & Schertler, G. F. (1998). Characterisation of an improved two-dimensional $p22_12_1$ crystal from bovine rhodopsin. *J. Mol. Biol.* **282**, 991-1003.

Luecke, H., Schobert, B., Richter, H.-T., Certailler, J.-P. & Lanyi, J. K. (1999). Structural changes in bacteriorhodopsin during ion transport at 2 Å resolution. *Science,* **286**, 255-260.

Mou, J. X., Yang, J. & Shao, Z. F. (1995). Atomic force microscopy of cholera toxin B-oligomers bound to bilayers of biologically relevant lipids. *J. Mol. Biol.* **248**, 507-512.

Müller, D. J. & Engel, A. (1997). The height of biomolecules measured with the atomic force microscope depends on electrostatic interactions. *Biophys. J.* **73**, 1633-1644.

Müller, D. J. & Engel, A. (1999). pH and voltage induced structural changes of porin OmpF explain channel closure. *J. Mol. Biol.* **285**, 1347-1351.

Müller, D. J., Schabert, F. A., Büldt, G. & Engel, A. (1995a). Imaging purple membranes in aqueous solutions at subnanometer resolution by atomic force microscopy. *Biophys. J.* **68**, 1681-1686.

Müller, D. J., Büldt, G. & Engel, A. (1995b). Force-induced conformational change of bacteriorhodopsin. *J. Mol. Biol.* **249**, 239-243.

Müller, D. J., Schoenenberger, C. A., Büldt, G. & Engel, A. (1996). Immuno-atomic force microscopy of purple membrane. *Biophys. J.* **70**, 1796-1802.

Müller, D. J., Amrein, M. & Engel, A. (1997). Adsorption of biological molecules to a solid support for scanning probe microscopy. *J. Struct. Biol.* **119**, 172-188.

Müller, D. J., Sass, H.-J., Müller, S., Büldt, G. & Engel, A. (1999a). Surface structures of native bacteriorhodopsin depend on the molecular packing arrangement in the membrane. *J. Mol. Biol.* **285**, 1903-1909.

Müller, D. J., Fotiadis, D., Scheuring, S., Müller, S. A. & Engel, A. (1999b). Electrostatically balanced subnanometer imaging of biological specimens by atomic force microscopy. *Biophys. J.* **76**, 1101-1111.

Müller, D. J., Heymann, J. B., Oesterhelt, F., Möller, C., Gaub, H., Büldt, G. & Engel, A. (2000). Atomic force microscopy on native purple membrane. *Biochim. Biophys. Acta,* in the press.

Müller, J., Münster, C. & Salditt, T. (2000). Thermal denaturating of bacteriorhodopsin by X-ray scattering from oriented purple membranes. *Biophys. J.* **78**, 3208-3217.

Neugebauer, D.-C., Zingsheim, H. P. & Oesterhelt, D. (1978). Recrystallization of the purple membrane *in vivo* and *in vitro*. *J. Mol. Biol.* **123**, 247-257.

Oesterhelt, D. (1973). Reversible dissociation of the purple complex in bacteriorhodopsin and identification of 13-*cis* and all-*trans*-retinal as its chromophores. *Eur. J. Biochem.* **40**, 453-463.

Oesterhelt, D. (1998). The structure and mechanism of the family of retinal proteins from halophilic archaea. *Curr. Opin. Struct. Biol.* **8**, 489-500.

Oesterhelt, D. & Stoeckenius, W. (1973). Functions of a new photoreceptor membrane. *Proc. Natl Acad. Sci. USA,* **70**, 2853-2857.

Oesterhelt, D. & Stoeckenius, W. (1974). Isolation of the cell membrane of *Halobacterium halobium* and its fraction into red and purple membrane. *Methods Enzymol.* **31**, 667-678.

Oesterhelt, D., Schuhmann, L. & Gruber, H. (1974). Light-dependent reaction of bacteriorhodopsin with hydroxylamine in cell suspensions of *Halobacterium halobium*: demonstration of an apo-membrane. *FEBS Letters,* **44**, 257-61.

Putman, C. A. J., van der Werft, K., de Grooth, B. G., van Hulst, N. F., Greve, J. & Hansma, P. K. (1992). A new imaging mode in atomic force microscopy based on the error signal. *Proc./Ser. Int. Soc. Opt. Eng. (SPIE),* **1639**, 198-204.

Sato, H., Takeda, K., Tani, K., Hino, T., Okada, T., Nakasako, M., Kamiya, N. & Kouyama, T. (1999). Specific lipid-protein interactions in a novel honeycomb lattice structure of bacteriorhodopsin. *Acta Crystallog. sect. D, Biol. Crystallog.* **55**, 1251-1256.

Saxton, W. O. & Baumeister, W. (1982). The correlation averaging of a regularly arranged bacterial cell envelope protein. *J. Microsc.* **127**, 127-138.

Saxton, W. O., Pitt, T. J. & Horner, M. (1979). Digital image processing: the semper system. *Ultramicroscopy,* **4**, 343-354.

Schabert, F. A., Henn, C. & Engel, A. (1995). Native *Escherichia coli* OmpF porin surfaces probed by atomic force microscopy. *Science,* **268**, 92-94.

Scheuring, S., Ringler, P., Borgina, M., Stahlberg, H., Müller, D. J., Agre, P. & Engel, A. (1999). High resolution topographs of the *Escherichia coli* water-channel aquaporin Z. *EMBO J.* **18**, 4981-4987.

Seelert, H., Poetsch, A., Dencher, N. A., Engel, A., Stahlberg, H. & Müller, D. J. (2000). Imaging the proton powered motor of chloroplast ATP synthase. *Nature,* **405**, 418-419.

Sternberg, B., Gale, P. & Watts, A. (1989). The effect of temperature and protein content on the dispersive properties of bacteriorhodopsin from *H. halobium* in reconstituted DMPC complexes free of endogenous purple membrane lipids: a freeze-fracture electron microscopy study. *Biochim. Biophys. Acta,* **980**, 117-126.

Subramaniam, S. (1999). The structure of bacteriorhodopsin: an emerging consensus. *Curr. Opin. Struct. Biol.* **9**, 462-468.

Subramaniam, S., Marti, T., Rosselet, S. J., Rothschild, K. J. & Khorana, H. G. (1991). The reaction of hydroxylamine with bacteriorhodopsin studied with mutants that have altered photocycles: selective reactivity of different photointermediates. *Proc. Natl Acad. Sci. USA,* **88**, 2583-2587.

Subramaniam, S., Lindahl, M., Bullough, P., Faruqi, A. R., Tittor, J., Oesterhelt, D., Brown, L., Lanyi, J. & Henderson, R. (1999). Protein conformational changes in the bacteriorhodopsin photocycle. *J. Mol. Biol.* **287**, 145-161.

Sumper, M. & Herrmann, G. (1976a). Biogenesis of purple membrane: regulation of bacteriorhodopsin. *FEBS Letters,* **69**, 149-152.

Sumper, M. & Herrmann, G. (1976b). Biosynthesis of purple membrane: control of retinal synthesis by bacterio-opsin. *FEBS Letters,* **71**, 333-336.

Unger, V. M., Hargrave, P. A., Baldwin, J. M. & Schertler, G. F. X. (1997). Arrangment of rhodopsin transmembrane α-helices. *Nature,* **389**, 203-206.

Walz, T., Tittmann, P., Fuchs, K. H., Müller, D. J., Smith, B. L., Agre, P., Gross, H. & Engel, A. (1996). Surface topographies at subnanometer-resolution reveal asymmetry and sidedness of aquaporin-1. *J. Mol. Biol.* **264**, 907-918.

White, S. H. & Wimley, W. C. (1999). Membrane protein folding and stability: physical principles. *Annu. Rev. Biophys. Biomol. Struct.* **28**, 319-365.

Yang, J., Tamm, L. K., Tillack, T. W. & Shao, Z. (1993). New approach for atomic force microscopy of membrane proteins. *J. Mol. Biol.* **229**, 286-290.

Edited by W. Baumeister

(Received 3 April 2000; received in revised form 17 June 2000; accepted 17 June 2000)